Supplementary material

Controlled Reconstruction of F-Doped NiFe-LDH into a Hierarchical Electrocatalyst for Saline Water Oxidation: Elucidating the Dual Role of Fluorine in Surface Stability and Active Phase Formation

Hossein Fattahimoghaddam [a,b,1], Chan-Yeup Chung [c,1], Ali Naderi[b] , Donghyeon Lee [b], Tae Kyu An [a,d], Jeong Ho Ryu [b*], Yong Jin Jeong [b*]*

[a] *Chemical Industry Institute, Korea National University of Transportation, Chungju, 27469, Republic of Korea*

[b] *Department of Materials Science and Engineering, Korea National University of Transportation, Chungju 27469, Republic of Korea*

[c] *Bio-Convergence R&D group, Korea Institute of Ceramic Engineering and Technology, Cheongju 28610, Republic of Korea*

[d] *Department of Polymer Science and Engineering, Korea National University of Transportation, Chungju 27469, Republic of Korea*

[*] ***Corresponding authors.***

E-mail addresses: taekyu1985@ut.ac.kr (Tae Kyu An), jhryu@ut.ac.kr (Jeong Ho Ryu), yjjeong@ut.ac.kr (Yong Jin Jeong)

[1] *These authors contributed equally*

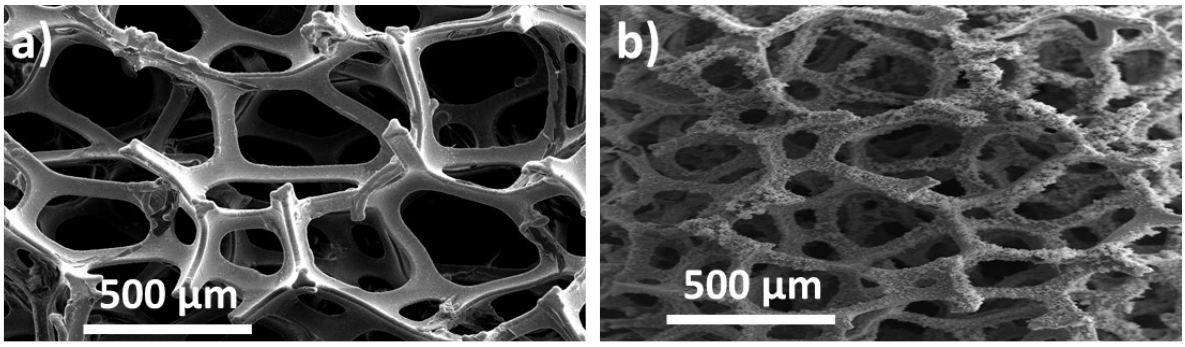

Fig. S1. SEM images of (a) bare NF, and (b) F-LDH/NF

Table S1. *Binding energy data, interpretations and atomic concentrations for the Fe 2p, Ni 2p, F 1s, O 1s spectra of all samples.*

	F-LDH/NF			**R-F-LDH/NF**		
XPS spectra	B.E. (eV)	Chemical state	Area (%)	B.E. (eV)	Chemical state	Area %
Fe 2P	706.11	Ni Auger	13307.55	706.04	Ni Auger	8887.344
	709.21	Fe(II)	15655.88	709.87	Fe(II)	10745.28
	711.43	Fe(III)	7960.389	711.62	Fe(III)	5860.869
	713.55	Ni Auger	9000.096	713.57	Ni Auger	6112.845
	715.91	Satellite	13009.16	715.96	Satellite	7256.754
	719.02	Satellite	14142.71	719.29	Satellite	5398.339
	724.64	Fe(II)	14722.25	724.95	Fe(II)	12280.11
Ni 2P	854.91	Ni-O	4416.564	854.89	Ni-O	22157.69
	856.29	Ni(II)	54955.66	855.99	Ni(II)	13680.87
	857.72	Ni(III)	42641.34	857.37	Ni(III)	12609.7
	860.68	Satellite	19723.66	860.56	Satellite	13715.65
	862.92	Satellite	24797.15	862.42	Satellite	8858.482
	864.56	Satellite	22693.89	864.4	Satellite	4894.701
	873.87	Ni(II)	27600.42	872.77	Ni(II)	11758.71
	875.6	Ni(III)	19049.5	874.54	Ni(III)	6819.38
	880.44	Satellite	46571.18	879.34	Satellite	20753.71
F 1s	683.74	Adsorbed F	17134.49	683.84	Adsorbed F	6606.856
	684.48	Doped F	7802.899	684.87	Doped F	3373.716
O 1s	531.08	Ni-O	5024.403	530.16	M-O	29531.69
	531.3	M-OH	19504.36	530.7	Ni-O	26610.78
	532.4	intercalated H_2O	30985.42	531.54	M-OH	11464.54
	533.11	Adsorbed H_2O	18367.85	532.2	intercalated H_2O	10436.78

Table S2. Comparison between activity and kinetic parameters of catalyst prepared at this work and previously reported catalysts.

No.	Compound	Overpotential (mV)	Electrolyte	Ref
1	Thin film Ni-Fe	η_{10}=280	1M KOH	[1]
2	Fe-Nioxy(hydroxide)	η_{10}=272	1M KOH	[2]
3	$Ni(OH)_2$/NiOOH	η_{10}=280	1M KOH	[3]
4	$Ni_{1-x}Fe_xOOH$	η_{10}=350	0.1M KOH	[4]
5	Fe0.1Ni0.9O	η_{10}=297	1M KOH	[5]
6	Co/Ni/4/1	η_{10}=336	1M KOH	[6]
7	Amorphous Ni-Fe layer hydroxide (a-NiFeO*x*H*y*)	η_{10}=270	0.1M KOH	[7]
8	HG-NiFe	η_{10}=310	1M KOH	[8]
9	Ni disk+Fe	η_{600}=400	1M KOH	[9]
10	Fe@ Ni nanofiber	η_{10}=230	1M KOH	[10]
11	$FeNiMoO_4$/ NF	η_{100}=257	1M KOH + 0.5M NaCl	[11]
12	Co-FeHy@NF	η_{10}=224	1M KOH + 0.5M NaCl	[12]
13	**R-F-LDH/NF**	**η_{10}=182 η_{100}=227**	**1M KOH + 0.5M NaCl**	**This work**

Supplementary Methods: Computational details

The density functional theory (DFT) calculations were conducted using the exchange-correlation energy function correlated by revised Perdew-Burke-Ernzerhof (RPBE) with the generalized gradient approximation (GGA) [13]. Self-consistent electronic density functional and total energy was obtained with the pseudopotential using the Vienna ab initio simulation package (VASP) code [14]. The plane wave basis set extended to 520 eV energy cutoff. Also, GGA+U correction scheme for transition metal cations such as Ni and Fe was adopted to correct energy of strongly correlated *3d* orbitals [15]. The Hubbard U values on Fe and Ni used in this calculation were 5.3 eV and 6.2 eV, respectively. The self-consistent loop was repeated until the total energy difference of systems between the adjacent repeating steps were less than 10^{-5} eV. To calculate wave functions only Γ-point was considered in irreducible Brillouin zone. The calculated slab models with the lowest surface energy of $Fe_{11}Ni_{21}(OH)_{64}$ (001) and $Fe_{11}Ni_{21}(OH)_{49}F_{15}$ (001) were generated to calculate surface OER reactions. Those slab models were optimized by conjugate-gradient method [16] with DFT-D3 Van der Waals energy correction [17] until the maximum Hellmann-Feynman force became in ±0.03 eV/Å. To incorporate implicit solvent effect in evaluating fluorine desorption energy for F-LDH surface, the dielectric constant for water 78.54 was used in VASPsol calculations [18].

The oxygen evolution reaction (OER) mechanism was modeled in alkaline media using a four-step proton–coupled electron transfer pathway:

(1) $*+OH^- \rightarrow {}^*OH+e^-$

(2) $*OH + *OH^- \rightarrow *O+H_2O+e^-$

(3) $*O+OH^- \rightarrow *OOH+e^-$

(4) $*OOH+OH^- \rightarrow *+O_2+H_2O+e^-$

Here, denotes an active site on the catalyst surface.

The Gibbs free energy change (ΔG) of each elementary step was calculated as:

$G_{*X}=E_{DFT}+E_{ZPE}-TS$

Where E_{DFT} is the total energy obtained from DFT calculations, E_{ZPE} is the zero-point energy correction, and TS represents the entropic contribution at room temperature (298 K).

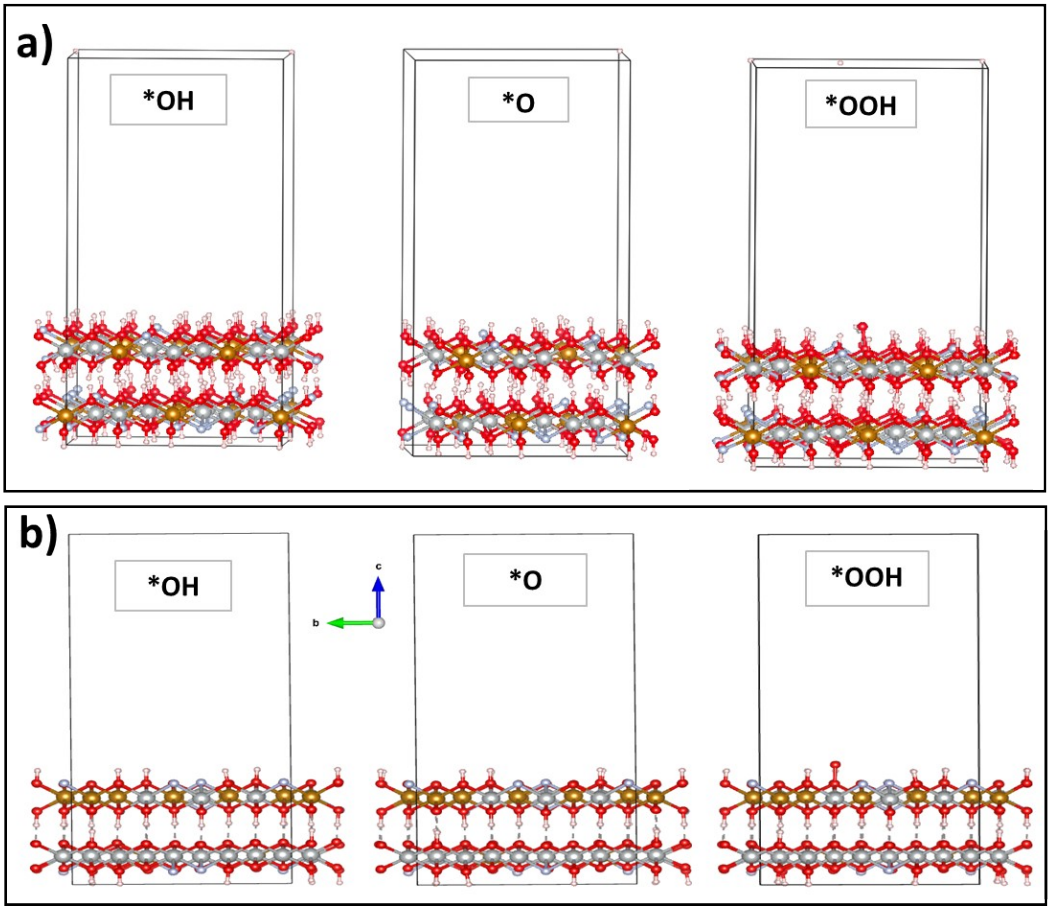

Fig. S2. The optimized adsorption configurations of the OER intermediates on (a) F-LDH (001) and (b) R-F-LDH surfaces. (The Fe and F substitution ratios in γ-NiOOH are based on XPS experimental results.)

Table S3. Calculated free energy steps for OER

Step	LDH (eV)	F-LDH (eV)	R-LDH (eV)	R-F-LDH (eV)
ΔG_1 (*OH)	0.311	-1.32	0.721	1.587
ΔG_1 (*O)	0.634	1.44	0.386	0.731
ΔG_1 (*OOH)	2.722	2.749	2.710	2.608
ΔG_1 (O_2)	1.246	2.036	1.096	0.287

Table S4. Calculated adsorption energy for Cl^-

Catalyst	E_{Cl^-+slab} (eV)	$E_{slab\ only}$ (eV)	E_{Cl^-} (eV)	Adsorption Energy (eV)
LDH	-830.85	-826.864	-4.847	**+0.861**

F-LDH	-740.247	-737.352	-4.847	**+1.952**
R-LDH	-662.011	-657.925	-4.847	**0.761**
R-F-LDH	-599.982	-596.056	-4.847	**0.921**

Table S5. Calculated fluorine vacancy formation energies for F-LDH in vacuum and aqueous environment.

Condition	**F-LDH with 1F vac. (eV)**	**F-LDH (eV)**	**1/2 * F_2 (eV)**	**Desorption Energy (eV)**
Vacuum	-731.137	-737.352	-1.660	**4.555**
H_2O implicit	-731.272	-736.651	-1.660	**3.720**

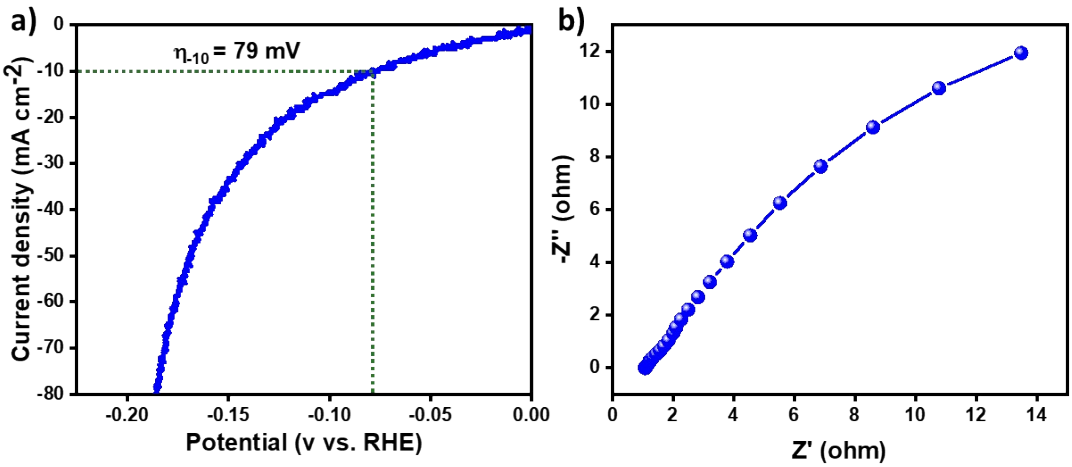

Fig. S3. (a) LSV curves for HER performance of F-LDH/NF (b) EIS Nyquist plots for F-LDH/NF

References

[1] M.W. Louie, A.T. Bell, An Investigation of Thin-Film Ni–Fe Oxide Catalysts for the Electrochemical Evolution of Oxygen, Journal of the American Chemical Society 135(33) (2013) 12329-12337.
[2] R.D.L. Smith, C. Pasquini, S. Loos, P. Chernev, K. Klingan, P. Kubella, M.R. Mohammadi, D. González-Flores, H. Dau, Geometric distortions in nickel (oxy)hydroxide electrocatalysts by redox inactive iron ions, Energy & Environmental Science 11(9) (2018) 2476-2485.
[3] S. Klaus, Y. Cai, M.W. Louie, L. Trotochaud, A.T. Bell, Effects of Fe Electrolyte Impurities on Ni(OH)2/NiOOH Structure and Oxygen Evolution Activity, The Journal of Physical Chemistry C 119(13) (2015) 7243-7254.
[4] D. Friebel, M.W. Louie, M. Bajdich, K.E. Sanwald, Y. Cai, A.M. Wise, M.-J. Cheng, D. Sokaras, T.-C. Weng, R. Alonso-Mori, R.C. Davis, J.R. Bargar, J.K. Nørskov, A. Nilsson, A.T. Bell, Identification of Highly Active Fe Sites in (Ni,Fe)OOH for Electrocatalytic Water Splitting, Journal of the American Chemical Society 137(3) (2015) 1305-1313.
[5] K. Fominykh, P. Chernev, I. Zaharieva, J. Sicklinger, G. Stefanic, M. Döblinger, A. Müller, A. Pokharel, S. Böcklein, C. Scheu, T. Bein, D. Fattakhova-Rohlfing, Iron-Doped Nickel Oxide Nanocrystals as Highly Efficient Electrocatalysts for Alkaline Water Splitting, ACS Nano 9(5) (2015) 5180-5188.
[6] X. Deng, S. Öztürk, C. Weidenthaler, H. Tüysüz, Iron-Induced Activation of Ordered Mesoporous Nickel Cobalt Oxide Electrocatalyst for the Oxygen Evolution Reaction, ACS Applied Materials & Interfaces 9(25) (2017) 21225-21233.
[7] H. Yin, L. Jiang, P. Liu, M. Al-Mamun, Y. Wang, Y.L. Zhong, H. Yang, D. Wang, Z. Tang, H. Zhao, Remarkably enhanced water splitting activity of nickel foam due to simple immersion in a ferric nitrate solution, Nano Research 11(8) (2018) 3959-3971.
[8] J. Wang, L. Gan, W. Zhang, Y. Peng, H. Yu, Q. Yan, X. Xia, X. Wang, In situ formation of molecular Ni-Fe active sites on heteroatom-doped graphene as a heterogeneous electrocatalyst toward oxygen evolution, Science Advances 4(3) eaap7970.
[9] L. Gong, J. Koh, B.S. Yeo, Mechanistic Study of the Synergy between Iron and Transition Metals for the Catalysis of the Oxygen Evolution Reaction, ChemSusChem 11(21) (2018) 3790-3795.

[10] J. Tao, Y. Zhang, S. Wang, G. Wang, F. Hu, X. Yan, L. Hao, Z. Zuo, X. Yang, Activating Three-Dimensional Networks of Fe@Ni Nanofibers via Fast Surface Modification for Efficient Overall Water Splitting, ACS Applied Materials & Interfaces 11(20) (2019) 18342-18348.
[11] J.-Y. Gao, Y.-L. Ma, G.-S. Qian, M.-Y. Si, L.-L. Han, J.-S. Li, Activating FeMoO 4 nanosheet arrays by partial nickel substitution for efficient electrocatalytic seawater oxidation, Chemical Communications 60(96) 14224-14227 (2024).
[12] H. Fattahimoghaddam, A. Naderi, D. Lee, S.-Y. Kweon, T.K. An, J.H. Ryu, Y.J. Jeong, Saline alkaline water splitting enabled by a Co3 + -rich iron hydroxide electrocatalyst: Advancing the water–energy nexus, Journal of Environmental Chemical Engineering 13(5) 117670 (2025).
[13] J.P. Perdew, K. Burke, M. Ernzerhof, Generalized gradient approximation made simple, Physical review letters 77(18) (1996) 3865.
[14] G. Kresse, J. Furthmüller, Efficient iterative schemes for ab initio total-energy calculations using a plane-wave basis set, Physical review B 54(16) (1996) 11169.
[15] L. Wang, T. Maxisch, G. Ceder, Oxidation energies of transition metal oxides within the GGA+ U framework, Physical Review B—Condensed Matter and Materials Physics 73(19) (2006) 195107.
[16] M.R. Hestenes, E. Stiefel, Methods of conjugate gradients for solving linear systems, Journal of research of the National Bureau of Standards 49 (1952) 409-435.
[17] S. Grimme, Semiempirical GGA-type density functional constructed with a long-range dispersion correction, Journal of computational chemistry 27(15) (2006) 1787-1799.
[18] K. Mathew, R. Sundararaman, K. Letchworth-Weaver, T. Arias, R.G. Hennig, Implicit solvation model for density-functional study of nanocrystal surfaces and reaction pathways, The Journal of chemical physics 140(8) (2014).